Optical Materials 37 (2014) 229–234

Contents lists available at ScienceDirect

Optical Materials

journal homepage: www.elsevier.com/locate/optmat

Polarized spectral properties of Sm^{3+}:$LiLuF_4$ crystal for visible laser application

G.Q. Wang [a,b], X.H. Gong [a], Y.F. Lin [a], Y.J. Chen [a], J.H. Huang [a], Z.D. Luo [a], Y.D. Huang [a,*]

[a] Key Laboratory of Optoelectronic Materials Chemistry and Physics, Fujian Institute of Research on the Structure of Matter, Chinese Academy of Sciences, Fuzhou, Fujian 350002, China
[b] University of Chinese Academy of Sciences, Beijing 100039, China

ARTICLE INFO

Article history:
Received 28 February 2014
Received in revised form 20 May 2014
Accepted 30 May 2014
Available online 18 June 2014

Keywords:
Sm^{3+}:$LiLuF_4$ crystal
Polarized spectral property
Visible laser application

ABSTRACT

A Sm^{3+}-doped $LiLuF_4$ single crystal was grown by the vertical Bridgman–Stockbarge technique. Polarized absorption spectra, polarized fluorescence spectra, and fluorescence lifetime of the Sm^{3+}:$LiLuF_4$ crystal were recorded at room temperature. Based on the Judd–Ofelt theory, spectral parameters of the Sm^{3+}:$LiLuF_4$ crystal were calculated. Emission cross sections for the $^4G_{5/2} \rightarrow {}^6H_J$ ($J = 5/2$, 7/2, 9/2, and 11/2) transitions with special interest for visible laser application were obtained by the Füchtbauer–Ladenburg formula. The results indicate that the Sm^{3+}:$LiLuF_4$ crystal may be a potential laser gain medium operating in visible region pumped by diode lasers around 401 nm.

1. Introduction

With the development of GaN laser diodes (GLD) in near ultraviolet to blue region, Compact all-solid state visible laser pumped by GLD has attracted many attentions for a variety of applications, such as color projection, high density optical data storage, laser printing, stereo lithography, argon-laser replacement, underwater communications, medicine, and photodynamic therapy.

GLD pumped solid-state visible lasers have been realized in recent years [1–4]. Among trivalent RE ions, the Sm^{3+} is one of the most interesting active ions for the visible lasers [5,6], which have been realized in Sm^{3+}-doped TbF_3 and $LiTbF_4$ crystals and silica glass fiber [7–9]. There are also several reports on Sm^{3+}-doped single crystals with potential for visible laser emission [10–14].

$LiLuF_4$ is isostructural with the uniaxial $LiYF_4$ crystal [15]. In the crystal, Lu^{3+} ions can be substituted by other trivalent rare-earth ions without charge compensation and lattice distortion. Like the $LiYF_4$, its negative thermal dependence of refractive index leads to weak overall thermal lensing and it also benefits from a closer match in its thermal expansion coefficient and conductivity along each of the crystal axes [16]. On the other hand, the $LiLuF_4$ grows congruently whereas the $LiYF_4$ grows incongruently, which means that the $LiLuF_4$ can be grown more easily because it does not need excess LiF, as in the case of $LiYF_4$, which could always create small inclusions in the crystal and reduce its optical quality. Therefore, laser operations have been achieved in Pr^{3+}, Nd^{3+}, Tm^{3+}, Ho^{3+}, and Yb^{3+}-doped $LiLuF_4$ crystals [17–21].

In this work, a Sm^{3+}-doped $LiLuF_4$ crystal is grown by the vertical Bridgman–Stockbarge technique. Room temperature polarized absorption and emission spectra are measured and analyzed in detail. Room temperature fluorescence decay curve of the $^4G_{5/2}$ multiplet of Sm^{3+} ions, which is the upper level of visible laser operation, is also measured. Then, the emission cross sections for the $^4G_{5/2} \rightarrow {}^6H_J$ ($J = 5/2$, 7/2, 9/2, and 11/2) transitions of Sm^{3+} ions, which are the main channels for visible lasers, are obtained by the Füchtbauer–Ladenburg (F–L) formula.

2. Experimental procedure

A single crystal Sm^{3+}:$LiLuF_4$ was grown by the vertical Bridgman–Stockbarge technique under Ar atmosphere. The concentration of Sm^{3+} ions in the crystal was measured to be 2.23 ± 0.05 at.% by the inductively coupled plasma atomic emission spectrometry (ICP-AES, Ultima2, Jobin–Yvon). One cuboid with dimensions of $5.0 \times 4.5 \times 4.0\ mm^3$ was cut from the as-grown crystal, and the optic axis is perpendicular to the face of $4.5 \times 4.0\ mm^2$. All the surfaces of the cuboid were polished for spectral experiments. All experiments were carried out at room temperature.

Polarized absorption spectra were recorded using a spectrophotometer (Lambda900, Perkin–Elmer) in a range of 270–1800 nm. Polarized fluorescence spectra in a range of 480–1300 nm were measured using a spectrometer (FL920, Edinburgh) equipped with a xenon lamp as the exciting source. Hamamatsu R955 and R5509

* Corresponding author. Tel.: +86 13959182610; fax: +86 591 83714946.
E-mail address: huyd@fjirsm.ac.cn (Y.D. Huang).

http://dx.doi.org/10.1016/j.optmat.2014.05.033
0925-3467/

photomultiplier tubes (PMTs) were used as the detectors in the VIS and NIR regions, respectively. A fluorescence decay curve of the $^4G_{5/2}$ multiplet was measured by another spectrometer (FLSP920, Edinburgh) equipped with a tunable mid-band optical parametric oscillator pulsed laser (~5 ns) (Vibrant 355II, OPOTEK) as the exciting source.

3. Results and discussion

3.1. Absorption spectra and Judd–Ofelt analysis

The room temperature absorption spectra were recorded in two principal polarizations, σ and π, which correspond to the electrical fields of the incident light perpendicular and parallel to the optic axis of the Sm^{3+}:$LiLuF_4$, respectively, and are presented in Fig. 1. Owing to the anisotropy of this uniaxial crystal, the spectra have strong polarization dependence. The absorption bands corresponding to the transitions from the ground multiplet $^6H_{5/2}$ to the excited multiplets of Sm^{3+} ions for each polarization are assigned by comparing the spectra with the previous data of Sm^{3+}:$LiYF_4$ (see Fig. 2) [22] and labeled by corresponding excited multiplets in Fig. 1. A number of absorption transitions with quartet terminal multiplets, including $^4G_{5/2,\ 7/2}$ and $^4F_{3/2}$, expected in the 500–600 nm region, are too weak to be discerned. The absorption band around 401 nm for the transition of $^6H_{5/2} \rightarrow {}^6P_{5/2}$ is important for the crystal which will be pumped by GLD as gain medium of visible laser. The peak cross sections are 1.51×10^{-20} and 1.04×10^{-20} cm^2 for π and σ polarizations, respectively, and both at 401 nm. They are smaller than the unpolarized 3.87×10^{-20} cm^2 at 408 nm and 2.44×10^{-20} cm^2 at 410 nm of Sm^{3+}:$GdVO_4$ and Sm^{3+}:YAP [12,23], respectively; but the peak cross section for π polarization of the Sm^{3+}:$LiLuF_4$ is larger than the 1.37×10^{-20} cm^2 at 401 nm of Sm^{3+}:$LiYF_4$ and the 1.07×10^{-20} cm^2 at 405 nm of Sm^{3+}:GGG crystal [10,24]. Full widths at half the maximum (FWHMs) of the absorption bands around 401 nm are about 2.3 nm for σ polarization and 3.1 nm for π polarization, which are comparable to the those for Sm^{3+}:$LiYF_4$, while the values for Sm^{3+}-doped GGG, $GdVO_4$ and YAP are 5, 8 and 8 nm, respectively [10,12,23].

Based on the polarized absorption spectra, spectral parameters of Sm^{3+} ion in $LiLuF_4$ were calculated by applying the Judd–Ofelt (J–O) theory [25,26], which has been widely used to calculate the line strengths of electric dipole (ED) transitions between multiplets for rare earth ions in solids. It should be noticed that transitions to some excited multiplets ($^6F_{3/2,\ 5/2}$, $^4G_{5/2,\ 7/2}$, $^4F_{3/2,\ 5/2}$, and $^4H_{7/2}$) fulfils the selection rules for magnetic dipole (MD) transitions $\Delta J = 0$, 1. The line strength of MD transition does not change with the host environment significantly and could be calculated using the formulas provided in Refs. [10,27]. The values of the reduced matrix

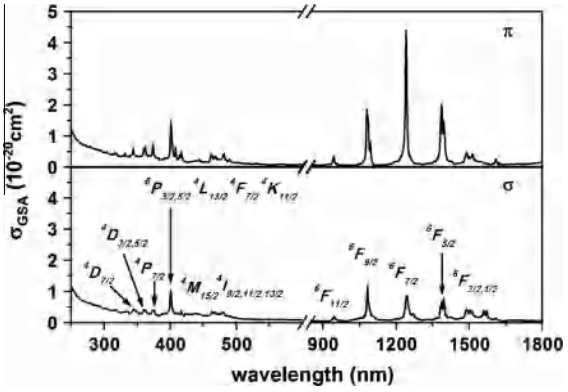

Fig. 1. Room temperature polarized absorption spectra of Sm^{3+}:$LiLuF_4$ crystal.

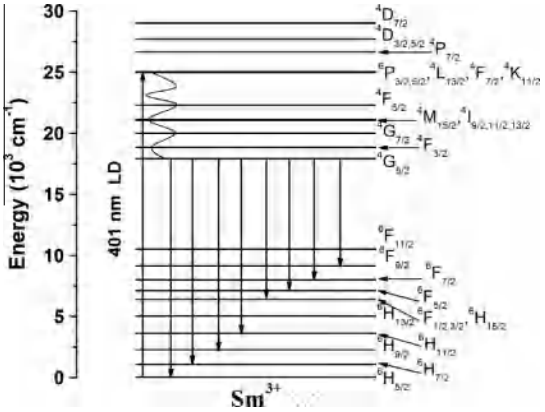

Fig. 2. Energy level scheme of Sm^{3+}.

elements of unit tensor operators were taken from Ref. [28]. The detailed calculation process can be found in Ref. [10]. The refractive indices n_q for σ and π polarization reported in Ref. [29] were used in the calculation. Three intensity parameters Ω_t ($t = 2, 4, 6$) were determined by a least square fitting between the experimental and theoretical line strengths. The average wavelength $\bar{\lambda}$, measured line strength S^{ED}_{exp}, and that calculated from the J–O intensity parameters S^{ED}_{cale} for each band are listed in Table 1. The root mean square (rms) error is defined as

$$\text{rms error}_q = \frac{\text{rms } \Delta S_q}{\text{rms } S_q} \times 100\%, \tag{1}$$

where rms ΔS_q is the root mean square deviation and

$$\text{rms } S_q = \sqrt{\sum_{i=1}^{M} S^2_{\text{exp},q}/M}, \tag{2}$$

in which M is the number of absorption bands adopted in the calculation. The values of rms ΔS_q and rms error_q are also listed in Table 1.

The effective J–O intensity parameters were calculated following $\Omega_{t,\text{eff}} = (2\Omega_{t,\sigma} + \Omega_{t,\pi})/3$ ($t = 2$, 4, 6) to facilitate comparison among different Sm^{3+}-doped materials [30]. The J–O intensity parameters of Sm^{3+}:$LiLuF_4$ and other Sm^{3+}-doped crystals are listed in Table 2 for comparison. The $\Omega_{2,\text{eff}}$ for Sm^{3+}:$LiLuF_4$ is larger than those for other Sm^{3+}-doped fluoride crystal, such as Sm^{3+}:K_2YF_5 and Sm^{3+}:$LiYF_4$, but smaller than those of Sm^{3+}-doped oxide crystals. One reason for the results is the stronger crystal field in the $LiLuF_4$ than those in other fluoride crystals [32]. Another is the weaker covalent bond of the Sm^{3+}-F than that of the Sm^{3+}-O [33–34].

From the polarized J–O intensity parameters, the ED spontaneous emission probability A^{ED}_q can be calculated. Taking the spontaneous emission probability of the MD transition A^{MD}_q into account, the average spontaneous emission probability can be calculated by $A = (2A_\sigma + A_\pi)/3$ with $A_q = A^{ED}_q + A^{MD}_q$. Then the fluorescence branching ratio β and the radiative lifetime τ_r can be further estimated. The results are listed in Table 3. The spontaneous emission probability of σ polarization is smaller than that of π polarization in visible region, hence visible laser with π polarization can be expected. Furthermore, the branching ratio for the $^4G_{5/2} \rightarrow {}^6H_{7/2}$ transition is the largest one and up to ~45%, so that Sm^{3+}:$LiLuF_4$ crystal is suitable for 600 nm laser emission.

3.2. Fluorescence spectra

Under excitation at 401 nm, namely exciting the Sm^{3+} ions to the $^6P_{5/2}$ multiplet, polarized fluorescence spectra in the ranges

Table 1
Mean wavelengths and experimental and calculated absorption line strengths of ED transitions of Sm^{3+}:$LiLuF_4$ crystal at room temperature.

$^6H_{5/2}\rightarrow$	$\bar{\lambda}$(nm)	σ Polarized $S(J\rightarrow J')$ (10^{-20} cm^2)		$\bar{\lambda}$(nm)	π Polarized $S(J\rightarrow J')$ (10^{-20} cm^2)	
		S^{ED}_{exp}	S^{ED}_{cale}		S^{ED}_{exp}	S^{ED}_{cale}
$^6F_{1/2,\ 3/2}$, $^6H_{15/2}$	1509.6	0.96	0.98	1527.0	0.87	0.89
$^6F_{5/2}$	1408.2	0.83	0.85	1392.3	1.52	1.38
$^6F_{7/2}$	1250.7	1.09	1.33	1245.9	2.22	2.25
$^6F_{9/2}$	1084.1	0.99	0.80	1084.5	1.33	1.34
$^6F_{11/2}$	953.7	0.13	0.12	956.6	0.18	0.19
$^4I_{9/2,\ 11/2,\ 13/2}$, $^4M_{15/2}$	472.5	0.17	0.16	478.4	0.48	0.26
$^4F_{5/2}$, $^4M_{17/2}$, $^4G_{9/2}$, $^4I_{15/2}$	437.9	0.04	0.02	441.5	0.07	0.04
(^6P, ^4P)$_{5/2}$, $^4L_{13/2}$,$^4F_{7/2}$, $^6P_{3/2}$, $^4K_{11/2}$, $^4L_{15/2}$, $^4G_{11/2}$	401.6	0.58	0.61	404.2	1.04	1.05
$^4D_{1/2}$, $^4P_{7/2}$, $^4L_{17/2}$, $^4K_{13/2}$	374.3	0.12	0.17	374.0	0.22	0.29
$^4F_{9/2}$, $^4D_{3/2,\ 5/2}$, $^6P_{5/2}$	361.5	0.13	0.12	361.6	0.19	0.20
$^4H_{7/2,\ 9/2,\ 11/2}$, $^4K_{15/2}$, $^4D_{7/2}$	345.6	0.13	0.09	344.1	0.15	0.15
rms ΔS(10^{-20} cm^2)		0.11			0.10	
rms error (%)		18.5			10.1	

Table 2
J–O intensity parameters for Sm^{3+}-doped crystals.

Crystal		Ω_2 (10^{-20} cm^2)	Ω_4 (10^{-20} cm^2)	Ω_6 (10^{-20} cm^2)	Refs.
Sm^{3+}:$LiLuF_4$	Ω_σ	1.76	2.79	2.17	This work
	Ω_π	0.66	4.77	3.65	
	Ω_{eff}	1.39	3.45	2.66	
Sm^{3+}:$LiYF_4$		0.55	2.44	1.72	[24]
Sm^{3+}:K_2YF_5		0.38	3.55	2.18	[31]
Sm^{3+}:GGG		3.90	2.48	1.83	[10]
Sm^{3+}:$CaNb_2O_6$		6.33	6.49	3.72	[13]

Table 3
Spontaneous emission probabilities, fluorescence branching ratios, and radiative lifetimes of Sm^{3+}:$LiLuF_4$ crystal.

Transition	$\bar{\lambda}_{em}$(nm)	$A^{ED}{}_\sigma$ (s^{-1})	$A^{MD}{}_\sigma$ (s^{-1})	$A^{ED}{}_\pi$ (s^{-1})	$A^{MD}{}_\pi$ (s^{-1})	A (s^{-1})	β (%)	τ_r(ms)
$^4G_{5/2}\rightarrow$								4.60
$^6F_{11/2}$	1395.0	0.18	0	0.29	0	0.22	0.10	
$^6F_{9/2}$	1185.3	0.96	0	0.68	0	0.86	0.40	
$^6F_{7/2}$	1043.7	1.63	0.94	2.64	0.90	2.90	1.33	
$^6F_{5/2}$	954.1	7.18	3.07	5.02	2.91	9.47	4.36	
$^6F_{3/2}$	910.1	1.05	4.51	0.54	4.28	5.32	2.45	
$^6H_{15/2}$	901.6	0.21	0	0.34	0	0.26	0.12	
$^6F_{1/2}$	890.2	0.89	0	0.32	0	0.70	0.32	
$^6H_{13/2}$	795.0	3.19	0	5.08	0	3.82	1.76	
$^6H_{11/2}$	713.0	19.12	0	30.84	0	23.03	10.59	
$^6H_{9/2}$	649.5	55.87	0	57.77	0	56.50	25.98	
$^6H_{7/2}$	600.7	71.91	10.78	115.17	10.23	96.92	44.57	
$^6H_{5/2}$	564.2	4.39	12.83	5.78	12.17	17.46	8.03	

of 450–800 nm and 800–1300 nm were recorded and are shown in Figs. 3 and 4, respectively. According to the energy level positions of Sm^{3+} ions in $LiYF_4$ crystal (see Fig. 2) [22], the emission bands around 564, 600, 650, and 713 nm are attributed to the $^4G_{5/2}\rightarrow{}^6H_J$ (J = 5/2, 7/2, 9/2, and 11/2) transitions, respectively, while the bands around 900, 1020, and 1160 nm are attributed to the $^4G_{5/2}\rightarrow{}^6F_{1/2,\ 3/2,\ 5/2}+{}^6H_{15/2}$, $^4G_{5/2}\rightarrow{}^6F_{7/2}$, and $^4G_{5/2}\rightarrow{}^6F_{9/2}$ transitions, respectively. The $^4G_{5/2}\rightarrow{}^6H_{7/2}$ emission with the most intense line around 600 nm is the possible channel for visible laser mentioned above.

It can be seen from Table 3 that the $^4G_{5/2}$ to ^6H_J (J = 9/2, 11/2, 13/2, and 15/2) and ^6F_J (J = 1/2, 9/2, and 11/2) are purely ED transitions but the $^4G_{5/2}$ to $^6H_{5/2,\ 7/2}$ and $^6F_{3/2,\ 5/2,\ 7/2}$ also obey MD transitions selection rule ΔJ = ±1, 0. The $^4G_{5/2}$ to $^6H_{5/2}$ and $^6F_{3/2}$ transitions are dominated by MD but the $^4G_{5/2}$ to $^6H_{7/2}$ is dominated by ED. These are in agreement with Ref. [24]. A MD transition does not change with the host environment significantly but an ED transition is sensitive to the crystal field. Therefore, as shown in Fig. 3 the intensities of the $^4G_{5/2}\rightarrow{}^6H_{5/2}$ transition for both polarizations are almost the same whereas the intensity of the $^4G_{5/2}\rightarrow{}^6H_{7/2}$ transition for π

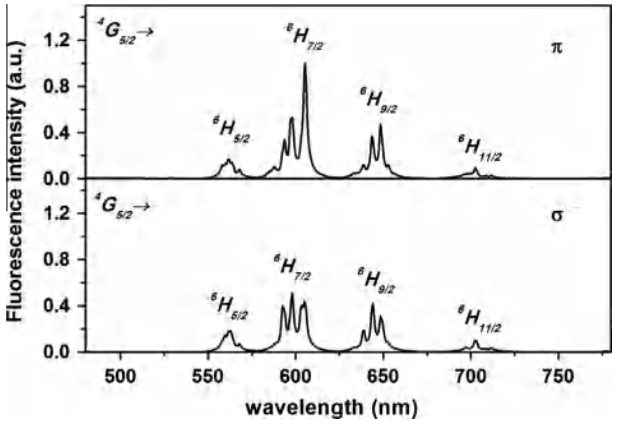

Fig. 3. Room temperature polarized fluorescence spectra of Sm^{3+}:$LiLuF_4$ crystal in visible region under excitation at 401 nm.

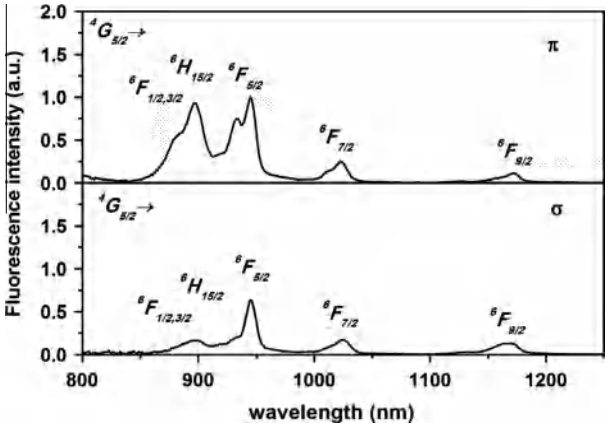

Fig. 4. Room temperature polarized fluorescence spectra of Sm^{3+}:$LiLuF_4$ crystal in infrared region under excitation at 401 nm.

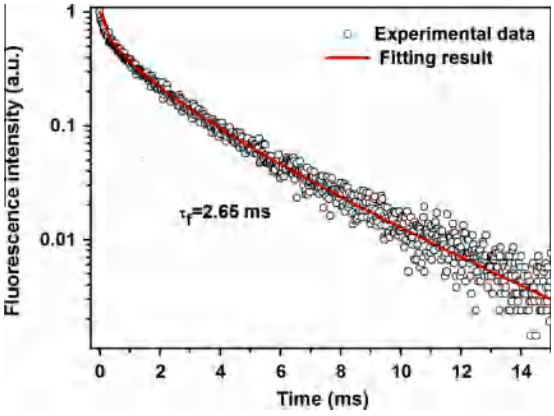

Fig. 5. Room temperature fluorescence decay curve of the $^4G_{5/2}$ multiplet of Sm^{3+}:$LiLuF_4$ crystal at 605 nm under excitation at 401 nm.

polarization is higher than that for σ polarization. These results are in agreement with the calculated emission probabilities listed in Table 3.

The stimulated emission cross sections for the $^4G_{5/2} \rightarrow {}^6H_J$ (J = 5/2, 7/2, 9/2, and 11/2) transitions can be calculated by the F–L formula [35]

$$\sigma_q^{em}(\lambda) = \frac{A_q \lambda^5 I_q(\lambda)}{8\pi c n_q^2 \int \lambda I_q(\lambda) d\lambda}, \tag{3}$$

where $I_q(\lambda)$ is the emission intensity at wavelength λ and c is the speed of light. The peak emission cross sections of the $^4G_{5/2} \rightarrow {}^6H_J$ (J = 5/2, 7/2, 9/2, and 11/2) transitions were calculated and are listed in Table 4. The largest cross-section is at 605 nm for π polarization and the value is 14.21 × 10^{-22} cm^2, which is smaller than those of Sm^{3+}-doped oxide crystals, such as the 31.7 × 10^{-22} cm^2 for Sm^{3+}:GGG, 35.4 × 10^{-22} cm^2 for Sm^{3+}:Gd_2SiO_5 and 17.2 × 10^{-22} cm^2 for Sm^{3+}:YAP [10,11,25]. However, it is larger than the 0.64 × 10^{-22} cm^2 for Sm^{3+}:K_2YF_5 and 10.39 × 10^{-22} cm^2 for Sm^{3+}:$LiYF_4$ [24,31].

3.3. Fluorescence dynamics

Fig. 5 shows the fluorescence decay curve of the $^4G_{5/2}$ multiplet for Sm^{3+}:$LiLuF_4$ recorded by measuring the emission of the $^4G_{5/2} \rightarrow {}^6H_{7/2}$ transition at 605 nm under excitation at 401 nm. It can be found that the decay of the $^4G_{5/2}$ multiplet is not single exponential, which generally implies that some energy transfer processes, such as the $^4G_{5/2} + {}^6H_{5/2} \rightarrow {}^6F_{11/2} + {}^6F_{5/2}$ and $^4G_{5/2} + {}^6H_{5/2} \rightarrow {}^6F_{7/2} + {}^6F_{9/2}$ denoted by (a) and (b) in Fig. 6, respectively, have influenced the decay of the $^4G_{5/2}$ multiplet [36,37].

In general, the energy-transfer process between activator ions becomes more frequent due to the distance between activator ions decreases as the activator concentration increases, which provides an extra decay channel. The non-exponential character of the fluorescence decay can be analyzed by the Inokuti–Hirayama (I–H) model [38], which assumes energy transfer from an excited Sm^{3+} donor to the surrounding Sm^{3+} acceptors in the ground state. According to this model, the fluorescence intensity can be described by

$$I(t) = I(0) \exp\left[-\frac{t}{\tau_0} - \Gamma\left(1 - \frac{3}{s}\right)\frac{N_0}{C}\left(\frac{t}{\tau_0}\right)^{\frac{3}{s}}\right], \tag{4}$$

where $I(t)$ is the fluorescence intensity at time t, τ_0 is the intrinsic fluorescence lifetime in the absence of the energy transfer, N_0 is the Sm^{3+} concentration expressed in ion/cm^3. $C = 3/4\pi R_c{}^3$ is the critical concentration related to the critical distance R_c defined as the distance at which the rate of energy transfer between the acceptor–donor pairs equals to the spontaneous decay rate of the excited donor, $\Gamma(x)$ is the gamma function evaluated in x, and s = 6, 8, and 10 correspond to the electric dipole–dipole, dipole–quadrupole, and quadrupole–quadrupole energy transfer mechanisms, respectively.

By the I–H model, the best fitting result of the experimental decay curve was obtained with s = 6. It indicates that the electric dipole–dipole energy transfer between Sm^{3+} ions is the dominate mechanism in the 2.23 at.% Sm^{3+}:$LiLuF_4$ crystal. The values of τ_0 and C for the crystal were fitted as 4.52 ms and 3.87 × 10^{20} cm^{-3}, respectively. Then, the critical distance R_c was derived as 0.85 nm. The average Sm–Sm distance in the crystal could be obtained from $R_{av} = (4\pi N_0/3)^{-1/3}$ and the value is 0.90 nm. The R_{av} of the 2.23 at.% Sm^{3+}:$LiLuF_4$ crystal is close to the R_c, which suggests that it is possible to find an acceptor inside the critical distance of an excited Sm^{3+} ion. The τ_0 is close to the τ_r in Table 3, which means that the multiphonon relaxation (MPR) rate from the $^4G_{5/2}$ multiplet to the next lower multiplet $^6F_{11/2}$ is negligible

Table 4
Peak fluorescence wavelengths, FWHMs, and stimulated emission cross sections σ^{em} of the transitions starting from the $^4G_{5/2}$ multiplet of Sm^{3+}:$LiLuF_4$ crystal.

Transition	Polarization	Peak wavelength (nm)	FWHM (nm)	σ^{em}(10^{-22} cm^2)
$^4G_{5/2}\rightarrow$				
$^6H_{11/2}$	σ	702.5	3.2	3.05
	π	702.0	5.2	5.26
$^6H_{9/2}$	σ	643.5	2.8	6.37
	π	648.5	7.2	7.82
$^6H_{7/2}$	σ	597.5	7.5	6.59
	π	605.0	9.5	14.21
$^6H_{5/2}$	σ	562.5	6.8	1.19
	π	561.5	7.8	1.18

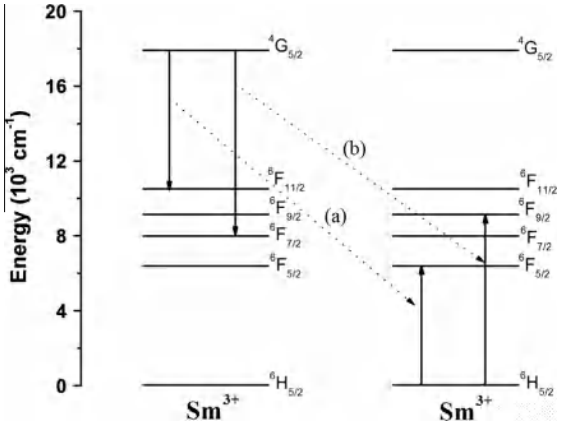

Fig. 6. Mechanisms of energy transfer between Sm^{3+}.

as there is a large energy gap of about 7000 cm^{-1} between them. Therefore, the electric dipole–dipole energy transfer between Sm^{3+} ions is the dominated nonradiative decay channel for the $^4G_{5/2}$ multiplet.

The average fluorescence lifetime τ_f of the $^4G_{5/2}$ multiplet could be obtained from the experimental decay curve by means of

$$\tau_f = \frac{\int_0^\infty tI(t)dt}{\int_0^\infty I(t)dt}, \quad (5)$$

The fluorescence lifetime of the $^4G_{5/2}$ multiplet was obtained to be 2.65 ms and shorter than the τ_0. It proves the existence of energy transfer related to the $^4G_{5/2}$ multiplet between Sm^{3+} ions in this 2.23 at.% Sm^{3+}:$LiLuF_4$ crystal. The fluorescence lifetime is longer than those of Sm^{3+}-doped oxide crystals, such as 2.1 ms for 0.56 at.% Sm^{3+}:GGG, 1.7 ms for 0.5 at.% Sm^{3+}:Gd_2SiO_5 and 0.55 ms for 2 at.% Sm^{3+}:$GdVO_4$ [10–12]. However, it is shorter than other Sm^{3+}-doped fluoride crystals, such as 4.8 ms for 1.0 at.% Sm^{3+}:K_2YF_5, 4.9 ms for 0.1 at.% Sm^{3+}:KY_3F_{10} and 4.8 ms for 0.52 at.% Sm^{3+}:$LiYF_4$ [24,31,39]. This is due to the stronger energy transfer in the $LiLuF_4$ crystal doped with higher concentration of Sm^{3+}. The quantum efficiency η ($\eta = \tau_f/\tau_r$) of the $^4G_{5/2}$ multiplet was estimated to be 57.6%, which is lower than Sm^{3+}:GGG (84%), Sm^{3+}:K_2YF_5 (93.6%) and Sm^{3+}:$LiYF_4$ (69%) [10,24,31]. The main reason for the lower quantum efficiency in the Sm^{3+}:$LiLuF_4$ than those in other oxide or fluoride crystals is the stronger cross relaxation caused by the higher concentration of Sm^{3+} ions in the crystal.

4. Conclusion

A 2.23 at.% Sm^{3+}-doped $LiLuF_4$ single crystal was grown by the vertical Bridgman–Stockbarge technique. The polarized absorption and emission spectra and the fluorescence decay curve of the $^4G_{5/2}$ multiplet were measured. The intensity parameters Ω_t (t = 2, 4, 6) have been evaluated based on the J–O theory, together with the radiative transition rates, the luminescent branching ratios, and the radiative lifetime of the $^4G_{5/2}$ multiplet. Cross relaxation dominates the non-radiative decay of the $^4G_{5/2}$ multiplet in this crystal. The critical distance R_c is about 0.76 nm. The fluorescence lifetime and quantum efficiency of the $^4G_{5/2}$ multiplet are 2.65 ms and 57.6%, respectively. The emission cross sections of the $^4G_{5/2} \rightarrow {}^6H_J$ (J = 5/2, 7/2, 9/2, and 11/2) transitions were calculated. The peak emission cross section at 605 nm for the Sm^{3+}:$LiLuF_4$ crystal is 14.39×10^{-22} cm^2 for π polarization. The results indicate that Sm^{3+}:$LiLuF_4$ crystal may be a potential visible laser material around 605 nm.

Acknowledgments

This work has been supported by the National Natural Science Foundation of China (Grant 91122033) and the Knowledge Innovation Program of the Chinese Academy of Sciences (Grant KJCX2-EW-H03-01).

References

[1] P. Camy, J.L. Doualan, R. Moncorge, J. Bengoechea, U. Weichmann, Diode-pumped Pr^{3+}:KY_3F_{10} red laser, Opt. Lett. 32 (2007) 1462.
[2] M. Fibrich, H. Jelínková, J. Šulc, K. Nejezchleb, V. Škoda, Visible cw laser emission of GaN-diode pumped Pr:$YAlO_3$ crystal, Appl. Phys. B 97 (2009) 363.
[3] T. Gün, P. Metz, G. Huber, Power scaling of laser diode pumped Pr^{3+}:$LiYF_4$ cw lasers: efficient laser operation at 522.6 nm, 545.9 nm, 607.2 nm, and 639.5 nm, Opt. Lett. 36 (2011) 1002.
[4] S.R. Bowman, S. O'Connor, N.J. Condon, Diode pumped yellow dysprosium lasers, Opt. Express 20 (2012) 12906.
[5] R.F. Wei, C.G. Ma, Y.L. Wei, J.Y. Gao, H. Guo, Tunable white luminescence and energy transfer in novel Cu^+, Sm^{3+} co-doped borosilicate glasses for W-LEDs, Opt. Express 20 (2012) 29743.
[6] H.N. Luitel, T. Watari, R. Chand, T. Torikai, M. Yada, Photoluminescence properties of a novel orange red emitting $Sr_4Al_{14}O_{25}$:Sm^{3+} phosphor and PL enhancement by Bi^{3+} co-doping, Opt. Mater. 34 (2012) 1375.
[7] B.N. Kazakov, M.S. Orlov, M.V. Petrov, A.L. Stolov, A.M. Tkachuk, Induced emission of Sm^{3+} ions in the visible region of the spectrum, Opt. Spectrosc. 47 (1979) 676.
[8] H.P. Jenssen, Advanced Solid State Lasers Technical Digest, ME2-1/73, Memphis, 1995.
[9] M.C. Farries, P.R. Morkel, J.E. Townsend, Samarium^{3+}-doped glass laser operating at 651 nm, Electron. Lett. 24 (1988) 709.
[10] W.P. Liu, Q.L. Zhang, D.L. Sun, J.Q. Luo, C.J. Gu, H.H. Jiang, S.T. Yin, Crystal growth and spectral properties of Sm:GGG crystal, J. Cryst. Growth 331 (2011) 83.
[11] A. Strzep, R. Lisiecki, P. Solarz, G. Dominiak-Dzik, W. Ryba-Romanowski, M. Berkowski, Optical spectra and excited state relaxation dynamics of Sm^{3+} in Gd_2SiO_5 single crystal, Appl. Phys. B 106 (2012) 85.
[12] X.M. He, L.H. Zhang, G.Z. Chen, Y. Hang, Crystal growth and spectral properties of Sm:$GdVO_4$, J. Alloys Comp. 467 (2009) 366.
[13] J.Q. Di, X.D. Xu, C.T. Xia, H.D. Zeng, Y. Cheng, D.Z. Li, D.H. Zhou, F. Wu, J.M. Cheng, J. Xu, Crystal growth and optical properties of Sm:$CaNb_2O_6$ single crystal, J. Alloys Comp. 536 (2012) 20.
[14] G. Dominiak-Dzik, Sm^{3+}-doped $LiNbO_3$ crystal, optical properties and emission cross-sections, J. Alloys Comp. 391 (2005) 26.
[15] I.A. Ivanova, A.N. Morozov, M.A. Petrova, I.G. Podkolzina, P.P. Feofilov, Preparation and properties of single crystals of double fluorides of lithium and the rare earths, Inorg. Mater. 11 (1975) 1868.
[16] F. Cornacchia, A. Toncelli, M. Tonelli, 2 μm Lasers with fluoride crystals: research and development, Prog. Quantum Electron. 33 (2009) 61.
[17] F. Cornacchia, A. Richter, E. Heumann, G. Huber, D. Parisi, M. Tonelli, Visible laser emission of solid state pumped $LiLuF_4$:Pr^{3+}, Opt. Express 15 (2007) 992.
[18] A.A. Kaminskii, K. Ueda, N. Uehara, H.R. Verdun, Room-temperature diode-laser-pumped efficient CW and Quasi-CW single-mode lasers based on Nd^{3+}-doped cubic disordered α-$NaCaYF_6$ and tetragonal ordered $LiLuF_4$ crystals, Phys. Status Solidi A 140 (1993) K45.
[19] N. Coluccelli, G. Galzerano, P. Laporta, F. Cornacchia, D. Parisi, M. Tonelli, Tm-doped $LiLuF_4$ crystal for efficient laser action in the wavelength range from 1.82 to 2.06 μm, Opt. Lett. 32 (2007) 2040.
[20] M. Schellhorn, A comparison of resonantly pumped Ho:YLF and Ho:LLF lasers in CW and Q-switched operation under identical pump conditions, Appl. Phys. B 103 (2011) 777.
[21] J.G. Yin, Y. Hang, X.M. He, L.H. Zhang, C.C. Zhao, J. Gong, P.X. Zhang, Direct comparison of Yb^{3+}-doped $LiYF_4$ and $LiLuF_4$ as laser media at room-temperature, Laser Phys. Lett. 9 (2012) 126.
[22] J.P.R. Wells, M. Yamaga, T.P.J. Han, H.G. Gallagher, M. Honda, Polarized laser excitation, electron paramagnetic resonance, and crystal-field analyses of Sm^{3+}-doped $LiYF_4$, Phys. Rev. B 60 (1999) 3849.
[23] Y.H. Zong, G.J. Zhao, J. Zhu, J. Xu, Growth and its spectroscopic properties of Sm:YAP crystal, J. Cryst. Growth 291 (2006) 468.
[24] G.Q. Wang, Y.F. Lin, X.H. Gong, Y.J. Chen, J.H. Huang, Z.D. Luo, Y.D. Huang, Polarized spectral properties of Sm^{3+}:$LiYF_4$ crystal, J. Lumin. 147 (2014) 23.
[25] B.R. Judd, Optical absorption intensities of rare-earth ions, Phys. Rev. 127 (1962) 750.
[26] G.S. Ofelt, Intensities of crystal spectra of rare-earth ions, J. Chem. Phys. 37 (1962) 511.
[27] M.J. Weber, Probabilities for radiative and nonradiative decay of Er^{3+} in LaF_3, Phys. Rev. 157 (1967) 262.
[28] C.K. Jayasankar, E. Rukmini, Optical properties of Sm^{3+} ions in zinc and alkali zinc borosulfate glasses, Opt. Mater. 8 (1997) 193.
[29] M.J. Weber, Handbook of Optical Materials, CRC Press, Boca Raton, 2003.
[30] Z.D. Luo, X.Y. Chen, T.J. Zhao, Judd–Ofelt parameter analysis of rare earth anisotropic crystals by three perpendicular unpolarized absorption measurements, Opt. Commun. 134 (1997) 415.

[31] P.V. Do, V.P. Tuyen, V.X. Quang, N.T. Thanh, V.T.T. Ha, N.M. Khaidukov, Y. Lee, B.T. Huy, Judd–Ofelt analysis of spectroscopic properties of Sm^{3+} ions in K_2YF_5 crystal, J. Alloys Comp. 520 (2012) 262.
[32] B.M. Walsh, N.P. Barnes, M. Petros, J. Yu, U.N. Singh, Spectroscopy and modeling of solid state lanthanide lasers: application to trivalent Tm^{3+} and Ho^{3+} in $YLiF_4$ and $LuLiF_4$, J. Appl. Phys. 95 (2004) 3255.
[33] W.F. Krupke, Optical absorption and fluorescence intensities in several rare-earth-doped Y_2O_3 and LaF_3 single crystals, Phys. Rev. 145 (1966) 325.
[34] R. Praveena, R. Vijaya, C.K. Jayasankar, Photoluminescence and energy transfer studies of Dy^{3+}-doped fluorophosphate glasses, Spectrochim. Acta, Part A 70 (2008) 577.
[35] Z.D. Luo, Y.D. Huang, X.Y. Chen, Spectroscopy of Solid-State Laser and Luminescent Materials, Nova Science, New York, 2007.
[36] P. Solarz, W. Ryba-Romanowski, Luminescence and energy transfer processes of Sm^{3+} in $K_5Li_2LaF_{10}$:Sm^{3+}-$K_5Li_2SmF_{10}$ single crystals, Phys. Rev. B 72 (2005) 075105.
[37] M. Malinowski, B. Jacquier, G. Boulon, W. Woliński, J. Lumin. 39 (1988) 301.
[38] M. Inokuti, F. Hirayama, Influence of energy transfer by the exchange mechanism on donor luminescence, J. Chem. Phys. 43 (1965) 1978.
[39] J.P.R. Wells, A. Sugiyama1, T.P.J. Han, H.G. Gallagher, Laser site selective excitation of KY_3F_{10}-doped with samarium, J. Lumin. 85 (1999) 91.